recycling

IMPACT FACTOR 4.6

CITESCORE 8.9

Article

An Integrated Leach–Extract–Strip Process for Yttrium Recovery from Spent Fluorescent Lamps: Kinetic Assessment and Solid–Liquid Extraction with D2EHPA-Impregnated XAD-7

Pedro Adrián Martínez-Montoya, Mónica Corea-Téllez, Ricardo Gerardo Sánchez-Alvarado, Teresita del Refugio Jiménez-Romero, Jorge Luis Gutiérrez-Estrada, Margarita García-Hernández and Angel de Jesús Morales-Ramírez

Topic
Converting and Recycling of Waste Materials

Edited by
Dr. Simeng Li and Dr. Tolulope A. Agunbiade

MDPI

https://doi.org/10.3390/recycling11010022

recycling

MDPI

Article

An Integrated Leach–Extract–Strip Process for Yttrium Recovery from Spent Fluorescent Lamps: Kinetic Assessment and Solid–Liquid Extraction with D2EHPA-Impregnated XAD-7

Pedro Adrián Martínez-Montoya [1], Mónica Corea-Téllez [1], Ricardo Gerardo Sánchez-Alvarado [2], Teresita del Refugio Jiménez-Romero [2], Jorge Luis Gutiérrez-Estrada [2], Margarita García-Hernández [3,4] and Angel de Jesús Morales-Ramírez [2,*]

[1] Escuela Superior de Ingeniería Química e Industrias Extractivas, ESIQIE-IPN, Laboratorio de Investigación en Polímeros y Nanomateriales, Unidad Profesional Adolfo López Mateos S/N Col. Lindavista, Gustavo A. Madero, Mexico City PC 07738, Mexico; pmartinezm1800@alumno.ipn.mx (P.A.M.-M.); mcorea@ipn.mx (M.C.-T.)

[2] Escuela Superior de Ingeniería Química e Industrias Extractivas, ESIQIE-IPN, Departamento de Ingeniería Metalúrgica Unidad Profesional Adolfo López Mateos S/N Col. Lindavista, Gustavo A. Madero, Mexico City PC 07738, Mexico; risanchez@ipn.mx (R.G.S.-A.); tjimenezr@ipn.mx (T.d.R.J.-R.); jgutierreze1401@alumno.ipn.mx (J.L.G.-E.)

[3] Instituto Politécnico Nacional, CECyT No. 16 "Hidalgo"-IPN, Carretera Pachuca—Actopan km 1+500, Distrito de Educación, Salud, Ciencia, Tecnología e Innovación, San Agustín Tlaxiaca PC 42162, Hidalgo, Mexico

[4] Instituto Politécnico Nacional, UPIIH-IPN, Carretera Pachuca—Actopan km 1+500, Distrito de Educación, Salud, Ciencia, Tecnología e Innovación, San Agustín Tlaxiaca PC 42162, Hidalgo, Mexico

* Correspondence: amoralesra@ipn.mx; Tel.: +52-57296000X55127

Abstract

Growing demand for rare earth elements (REEs) necessitates the development of efficient recycling strategies from secondary sources. This work presents a complete hydrometallurgical process for recovering yttrium (Y) from spent fluorescent lamps, emphasizing the efficient coupling of a conventional acid leaching with a solid–liquid extraction system. Multi-stage sulfuric acid leaching (2 M, 65 °C, an S/L ratio of 0.25 g/L) achieved a cumulative yttrium dissolution of 71.11% over four stages, with individual stage recoveries (based on initial yttrium content) of 44.2%, 21.56%, 7.19%, and 0.68%. Kinetic and spectroscopic analyses (FTIR, SEM-EDS) revealed that the leaching rate is controlled by diffusion through an in situ formed sulfate-rich layer ($CaSO_4$, Na_2SO_4), as described by the Z-L-T (Zhuravlev–Leshokin–Templeman) model (Ea = 35.5 kJ mol^{-1}). The resulting leachate was subjected to solid–liquid extraction using Amberlite XAD-7 resin impregnated with D_2EHPA. Under optimal conditions, the extraction process was highly efficient, yielding over 99% yttrium recovery at an optimal pH of 0.75 with a low resin dosage of 0.1 g/L. Furthermore, the solvent-impregnated resins exhibited excellent reusability over five consecutive extraction–stripping cycles, maintaining a single-cycle stripping efficiency above 70% and a cumulative recovery exceeding 97%. This study validates the technical feasibility of an integrated leach–extract–strip process based on impregnated resins as an alternative approach for yttrium recycling from electronic waste, potentially supporting the development of a circular economy.

Keywords: yttrium recovery; solid–liquid extraction; XAD-7 resin; fluorescent lamp recycling; leaching kinetics

Check for updates

Academic Editors: Ana Paula Paiva, Simeng Li and Tolulope A. Agunbiade

Received: 3 October 2025
Revised: 12 January 2026
Accepted: 14 January 2026
Published: 19 January 2026

 https://doi.org/10.3390/recycling11010022

1. Introduction

Rare earth elements (REEs) are a group of strategic metals that includes scandium (Sc), yttrium (Y), and the fifteen lanthanides located in the 4f block of the periodic table that are considered strategic materials due to their critical role in advanced technologies. These elements share similar electronic and chemical properties, making their separation and purification challenging [1]. From a chemical perspective, the lanthanides are commonly classified into light rare earth elements (LREEs), or the cerium group, which includes Sc, and heavy rare earth elements (HREEs), or the yttrium group [1,2].

REEs are found in a variety of minerals, occurring in both primary and secondary deposits. However, their concentration in most rock-forming minerals is not economically feasible for direct exploitation [3]. Furthermore, their mineralogical distribution varies significantly depending on the geology of the deposit. These elements are essential in high-value technological applications, such as wind turbines, batteries for electric vehicles, electronic displays, fluorescent lamps, and wear-resistant materials [4].

Increased generation of waste electrical and electronic equipment has driven the development of urban mining strategies to recover REEs from technological waste. Since 2011, international organizations have recognized the recycling of waste electrical and electronic equipment as a socioeconomic priority [3,5]. This approach offers multiple benefits, such as a reduced environmental impact, enhanced supply security of critical materials, and the creation of circular value chains [3].

Among the most established recycling processes is that for fluorescent lamps. Fluorescent lamp dust contains over 50 metallic and non-metallic components, including REE-rich phosphors, such as europium (Eu), terbium (Tb), and yttrium (Y), with the latter being the most abundant [6]. Tens of millions of these lamps are discarded each year, representing a major environmental challenge [4,5,7]. Although components such as glass, metals, and polymers can be recycled, phosphors containing rare earths often are not recovered and end up in landfills.

Although different methods have been proposed for the recovery of these materials, most involve the use of strong acids, such as hydrochloric acid [8,9] or nitric acid [10]. This generates large volumes of aqueous waste that then require treatment [11]. The recovery processes for yttrium, europium, and other REE require a secondary refining step. Among the secondary processes following leaching, the use of phosphinic acid and phosphinate-based extractants, such as the Cyanex 272 and Cyanex 572 families, has frequently been reported for REE extraction [12]. The use of this type of extractant in liquid–liquid extraction processes has significant disadvantages, such as the formation of a third phase, requiring the use of a phase modifier during the extraction process, a strong dependence on aliphatic diluents (e.g., kerosene), and highly controlled pH conditions that require additional refining stages during extraction [12,13].

In comparison, D_2EHPA (di-(2-ethylhexyl) phosphoric acid) has been reported as an efficient extractant for different trivalent rare earths (TRs), with particular affinity for the recovery of Y [14], as it requires fewer additives and allows for better pH control [9,15]. To overcome several operational drawbacks associated with liquid–liquid extraction, the solid–liquid extraction approach using solvent-impregnated resins (SIR's) can be considered, as it increases the contact area, prevents third-phase formation, and can enhance recovery efficiency [16].

The solid–liquid extraction process requires a suitable porous support material. In the last decade, the use of such support materials for solid–liquid extraction processes has gained importance due to the advantages they offer [17,18], including increased contact area and more efficient use of the extractant without the formation of a third phase. Support

https://doi.org/10.3390/recycling11010022

materials are used as a base for impregnation with extractants such as Cyanex-272, Cyanex-572, D_2EHPA (DEHPA), P227, TOPO, TBP, Cyanex-923, and Aliquat-336 [19].

The most reported advantages of using XAD-7 as a support material are high selectivity (depending on the extractant), ease of batch operation, and reduced secondary residues compared to liquid–liquid extraction. It supports multiple adsorption–desorption cycles and can operate in acidic, nitric, or hydrochloric matrices, depending on the system [19,20]. Some frequently reported disadvantages are low capacity per gram (usually lower than that of highly functionalized chelating compounds or inorganic materials), risk of extractant loss, heterogeneity in impregnation (distribution of extractant within the pores), heterogeneity in particle size, mass transfer limitations (intraparticle diffusion), and pH sensitivity that affects selectivity [19–21]. Table 1 summarizes reports on the efficiency of using XAD-7 resins for the extraction of different metals.

Table 1. Comparison of XAD-7 and other resins for metal extraction.

Year	Resin/Support Material	Extractant	Recovery/Capacity/Stripping/ Highlights	Reference
2004	Amberlite XAD-7	DEHPA, Ionquest-801, Cyanex-272	Pb(II) extraction efficiency 95% under optimal pH for DEHPA.	[22]
2007	Amberlite XAD-7	D_2EHPA	Kinetic diffusion coefficient ~10^{-12} m^2/s; high adsorption under optimal conditions.	[23]
2011	Amberlite XAD-7	D_2EHPA	Arsenate (As(V)) removal; equilibrium, kinetic, and thermodynamic modeling.	[24]
2018	Amberlite XAD-7	Cyanex-272	Equilibrium capacities: La 11.1 mg/g, Pr 0.56 mg/g, Nd 1.69 mg/g, Sm 0.75 mg/g, Eu 0.10 mg/g, Gd 0.25 mg/g; stripping with 0.1 M HNO_3: 100% Pr, Nd, Gd; 95.1% Eu.	[25]
2018	Amberlite XAD-7	Dibenzo-18-crown-6+ Fe(III)	Maximum As(V) adsorption: 18.8 µg As(V)/g resin; fits Sips isotherm, pseudo-2nd-order kinetics; reusable for ~5 cycles.	[26]
2021	* Amberlite XAD-16	Chelating groups (amidino-thiourea)	Reported removal of Cd(II) and Pb(II); high capacity.	[27]
2021	Amberlite XAD-7	Dibenzo-18-crown-6 (DB18C6)	For $\mathrm{Pd(II)} : q_{max} = 6.5$ mg Pd(II)/g resin; adsorption increases with temperature (0.83–3.05 mg/g from 298 to 328 K).	[28]
2023	Amberlite XAD-7	Cyanex-272	$\mathrm{Ce(III)}$ recovery : 99.75%; $\mathrm{La(III)}$: 69.98%. q_{max} Ce = 11.873 mg/g, La = 7.324 mg/g.	[29]
2024	Amberlite XAD-7	DL-valine (amino acid)	Novel material, SIR method with DL-valine.	[30]
2024	Amberlite XAD-7	D_2EHPA	Proposed yttrium extraction process applying solid–liquid extraction. 80% extraction while 75% stripping.	[14]

* not XAD-7, but related family.

While the individual steps of sulfuric acid leaching and D_2EHPA-based extraction are well-documented, their effective integration and systematic evaluation for the specific case of complex fluorescent lamp waste leachates represent a practical engineering challenge. Furthermore, detailed kinetic studies, alongside a complete process flow assessment (leaching, extraction, stripping, resin reusability) for this waste stream, are not extensively reported.

Therefore, this work focuses on the systematic evaluation and integration of a hydrometallurgical process for yttrium recovery from spent fluorescent lamps. The study aims first to optimize sulfuric acid leaching conditions (including solid–liquid ratio, acid concentration, and temperature) and to elucidate the associated leaching kinetics and mechanism. Subsequently, it evaluates the performance of D_2EHPA-impregnated Amberlite XAD-7 resin for the solid–liquid extraction of yttrium from the resulting complex leachate by determining the optimal pH and resin dosage, while directly comparing its efficiency with conventional liquid–liquid extraction. Furthermore, the reusability of the solvent-impregnated resin is assessed over multiple consecutive extraction–stripping cycles. Finally, a preliminary techno-economic analysis of the fully integrated process is provided. The primary contribution of this study lies in the comprehensive demonstration and validation of this integrated leach–extract–strip process for a real-world waste matrix, thereby supporting its potential implementation within a circular economy framework for rare earth elements.

2. Results and Analysis

2.1. Waste Chemical Characterization

A structural characterization was performed using X-ray diffraction (XRD) on both the total ground waste material and the phosphor powder isolated from the glass matrix through density separation. The corresponding diffractograms are presented in Figure 1. The XRD pattern of the total waste material exhibited only a broad band from 15° to 30°, characteristic of an amorphous structure, confirming that the glass substrate of the lamp constitutes the largest mass fraction of the recyclable material. In contrast, the phosphor powder pattern revealed a complex mixture of crystalline phases. The identified compounds included yttrium oxide doped with europium ($Y_2O_3:Eu^{3+}$, ICDD 00-025-1011), lanthanum-cerium-terbium phosphate ($La_{0.43}Ce_{0.44}Tb_{0.13}PO_4$, ICDD 01-078-6321), barium magnesium aluminate doped with europium ($BaMgAl_{10}O_{17}:Eu^{2+}$, ICDD 00-001-072-6158), cerium phosphate ($CePO_4$, ICDD 00-032-0199), and lanthanide phosphate ($LnPO_4$, ICDD 00-035-0731). The presence of these phases is directly linked to the function of the lamp, where the combination of blue ($BaMgAl_{10}O_{17}:Eu^{2+}$), green((La,Ce,Tb)$PO_4$), and red ($Y_2O_3:Eu^{3+}$) emitters produces white light. The dominance of $Y_2O_3:Eu^{3+}$ as the major crystalline phase is particularly significant for resource recovery. Given that yttrium is a critical REE with high economic value, this fraction is the primary target for hydrometallurgical recovery.

The chemical analysis of the fluorescent lamp waste powder was determined by X-ray fluorescence (XRF). The results, shown in Table 2 for the principal elements and oxides, revealed a complex inorganic matrix primarily composed of silicon (30.60% as SiO_2), aluminum (21.40% as Al_2O_3), and calcium (15.90% as CaO). This composition is consistent with the glass constituents and other phosphor components commonly found in fluorescent lamps. Critically for this study, the yttrium was directly quantified at a low concentration of 0.442 wt. %, confirming its status as a valuable but minor component within the waste stream. This complex chemical matrix underscores the technical and economic challenge of recovering this critical REE and justifies the need for the highly efficient leaching and solid–liquid extraction process developed here to achieve viable recovery rates.

https://doi.org/10.3390/recycling11010022

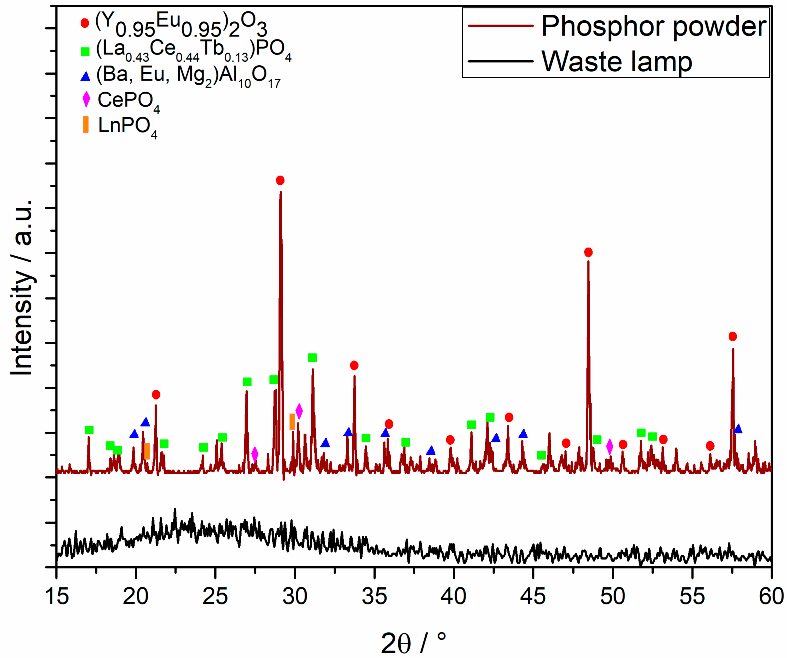

Figure 1. X-ray diffraction (XRD) patterns of total fluorescent lamp waste and isolated phosphor powder.

Table 2. Chemical composition of waste lamps by XRF.

Element	Wt./%	Oxide	Wt./%
Ca	20.40	SiO_2	30.60
Na	20.40	Al_2O_3	21.40
Si	18.90	CaO	15.90
Al	14.80	P_2O_5	14.30
P	8.54	Na_2O	13.90
Mg	1.76	SO_3	0.77
Sr	1.37	TiO_2	0.48
K	0.62	K_2O	0.41
Mn	0.42	MnO	0.40
Fe	0.34	Fe_2O_3	0.29
Ti	0.28		
Hg	0.11		

Loss on ignition (LOI) tests were conducted to quantify the content of volatile and organic matter. The very low mass loss observed (LOI = 0.42%) confirms that the material is predominantly inorganic in nature, with the minor weight loss primarily attributed to polymeric binders and residual organic compounds associated with the phosphor coating.

2.2. Waste Leaching

The leaching of powders obtained from ground electronic waste was performed using H_2SO_4. Sulfuric acid was selected over organic acids (e.g., citric, oxalic, or ascorbic acids) due to the slower leaching kinetics typically observed with such alternatives [31]. Additionally, H_2SO_4 is preferred over HCl or HNO_3 due to its greater availability, lower cost, reduced risk of equipment corrosion, and ease of neutralization. Its effectiveness in REE leaching has also been widely demonstrated [32–34]. The dissolution of yttrium oxide in sulfuric acid yields a ΔG° of −24.2 kJ/mol, confirming that the reaction is spontaneous under standard conditions according to Equation (1):

$$Y_2O_3 + 3H_2SO_4 \rightarrow Y_2(SO_4)_3 + 3H_2O \quad \Delta G^{\circ} = -24.2\, kJ/mol, \quad k \tag{1}$$

This reaction produces water-soluble yttrium sulfate ($Y_2(SO_4)_3$), releasing Y^{3+} ions into the aqueous phase, which is a highly favorable process, as demonstrated by the markedly negative ΔG° of −427.0 kJ/mol, indicating that $Y_2(SO_4)_3$(s) can dissociate in aqueous solution, as shown in Equation (2):

$$Y_2(SO_4)_3 \rightarrow 2Y^{3+} + 3SO_4^{2-}\ \Delta G^{\circ} = -427.0\, kJ/mol \tag{2}$$

Complete digestion of fluorescent lamp waste was performed using a mixture of hydrochloric and nitric acids. The results are shown in Table 3. Other REEs typically found in lamps were observed, but in much smaller proportions than yttrium; these could be removed during the leaching process. Therefore, it was decided to focus on improving the efficiency of yttrium release by modifying the acid concentrations used and by controlling the secondary extraction process by means of pH.

Table 3. Rare earth element content in fluorescent lamps.

Element	mg/kg	Element	mg/kg
Y	4229	Ca	8048
Ce	5781	Na	7408
Eu	4957	Sr	1909
Tb	2797	Mg	488
Gd	1638	Al	535

The effects of the solid–liquid ratio (S/L: 0.5 and 0.25 g/L) and H_2SO_4 concentration (1 M and 2 M) on the leaching efficiency at room temperature are shown in Figure 2a,b. After 300 min, the maximum recovery efficiency (26.1%) was achieved under the highest acid concentration (2 M) and the lowest S/L ratio (0.25 g/L). Lower S/L ratios improved recovery at both acid concentrations, as the reduced solid content increases the collision frequency between particles and acid molecules, thereby enhancing dissolution. Similarly, higher H_2SO_4 concentrations accelerated yttrium recovery.

Temperature significantly influences the leaching kinetics by increasing the reaction rates. Isothermal leaching experiments were conducted at S/L = 0.25 g/L and 2 M H_2SO_4 (Figure 3). As anticipated, the yttrium recovery increased with temperature, reaching 33.5%, 36.1%, 39.6%, and 44.2% at 35, 45, 55, and 65 °C, respectively. To further analyze leaching variables and dissolution mechanisms, kinetic modeling was performed. No leaching experiments were conducted at higher temperatures, as the objective was to conserve energy and minimize leaching agent losses due to evaporation.

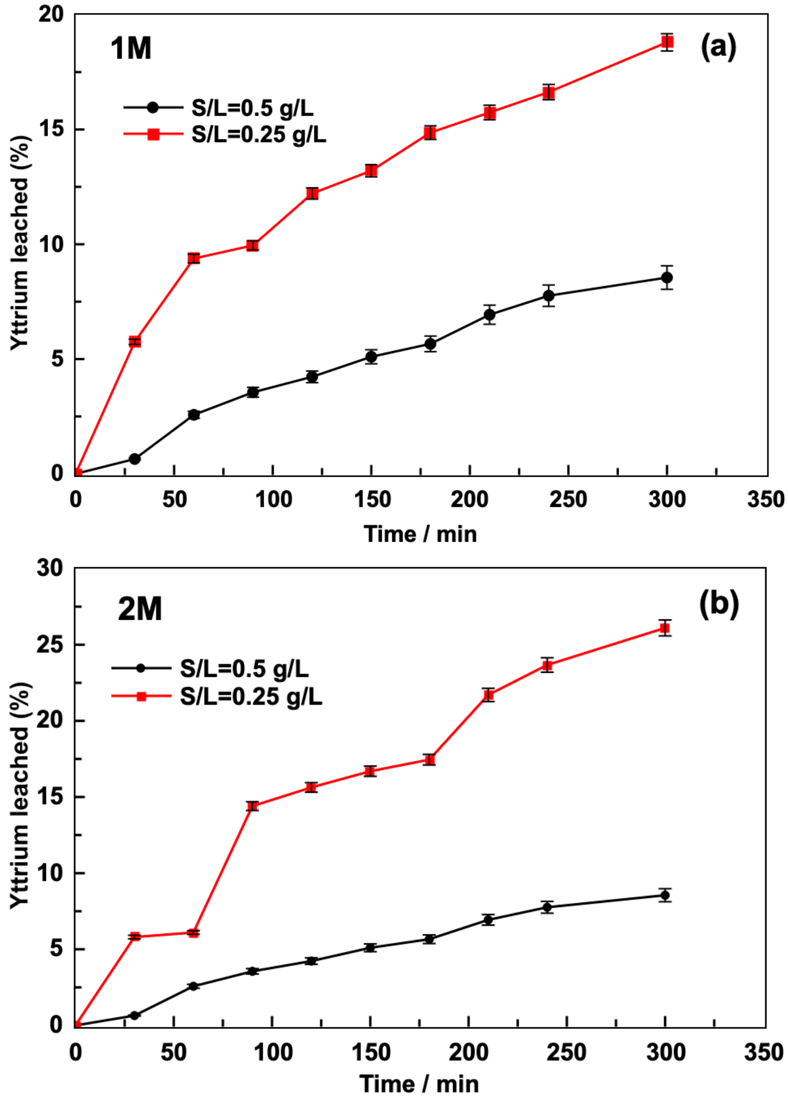

Figure 2. Effect of solid–liquid ratio on yttrium recovery first-cycle leaching kinetics: (**a**) 1 M H_2SO_4, (**b**) 2 M H_2SO_4.

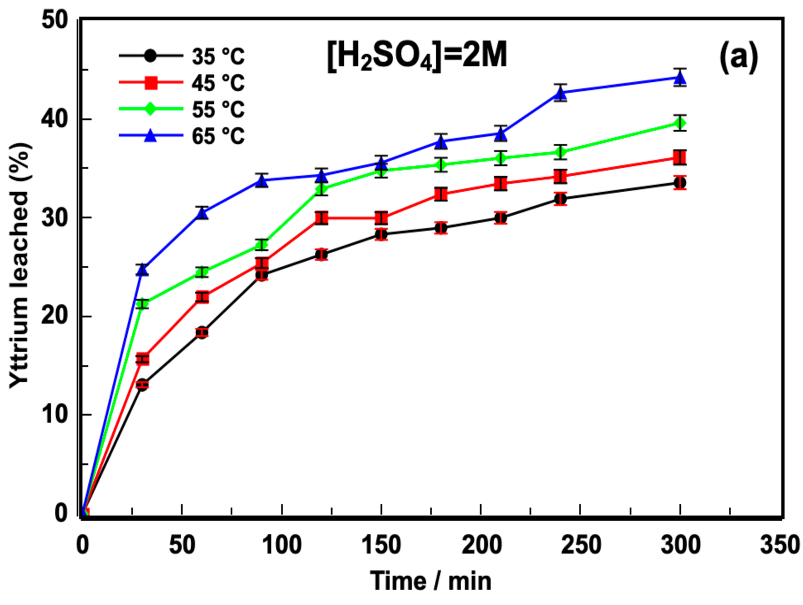

Figure 3. *Cont.*

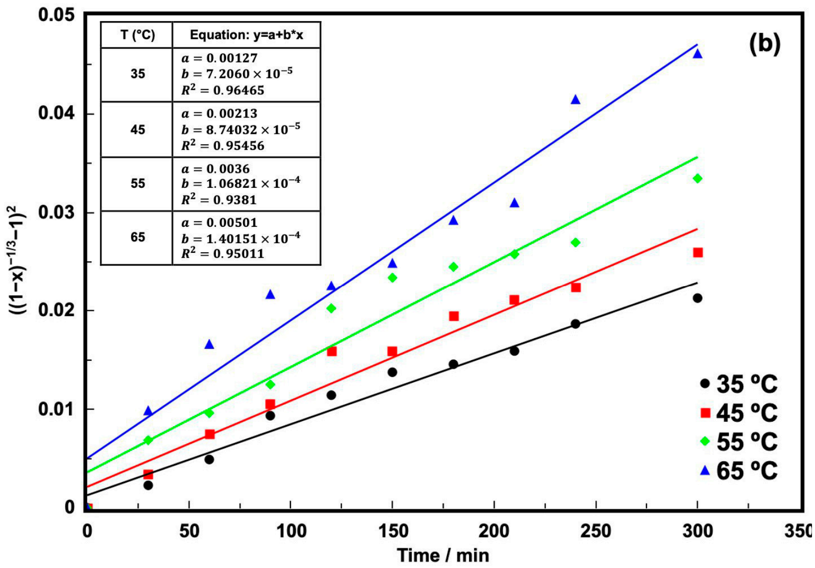

Figure 3. (**a**) Leaching kinetics of yttrium as a function of temperature, first cycle at S/L = 0.25 g/L and 2 M H_2SO_4. (**b**) Z-L-T model.

2.2.1. Batch Leaching

The cyclic leaching process was performed to increase the yttrium recovery. The optimal conditions were 65 °C, 2 M H_2SO_4, and an S/L of 0.25 g/L. The results are shown in Figure 4 and Table 4. Two stages were sufficient to achieve more than 65% yttrium release, and four stages achieved 71.11% release. This multi-cycle approach is standard in industrial hydrometallurgical operations, as it balances reagent consumption with metal recovery while generating leachates compatible with solvent extraction. Furthermore, the recovery achieved through four cycles demonstrates the scalability and practicality of the process, avoiding the operational and environmental drawbacks associated with single-stage, high-acid leaching.

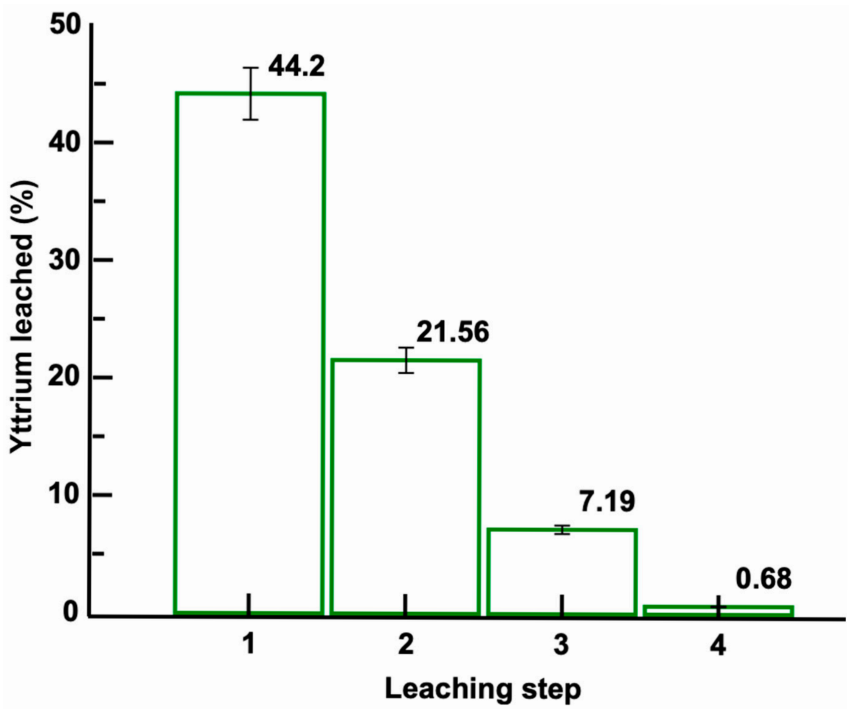

Figure 4. Batch leaching for yttrium recovery by cycle: 2 M H_2SO_4, S/L = 0.25 g/L, 65 °C, 300 min by cycle. The initial yttrium content before the first leaching cycle has been used as the basis for calculation.

Table 4. Batch leaching for the recovery of yttrium from an initial base concentration: ~1058 mg.

Leaching Step	Process Time	S-L	% Leaching	Efficiency per Step	% Remaining	% Accumulative Recovery	[Y] (mg/L)	Concentration per Step per Litter of Total Acid Used (mg/L)
1	300 min	0.25 g/L	44.20	44.20	55.80	44.20	461.90	461.90
2			21.56	48.77	34.24	64.76	233.54	347.72
3			7.19	33.34	27.05	72.95	77.94	257.79
4			0.68	9.45	26.37	73.63	7.42	195.20
Total % extraction after 4 steps							73.63%	
Total yttrium concentration after 4 cycles						195.20 mg/L		

2.2.2. Kinetic Modeling

The leaching kinetics of yttrium-containing waste with H_2SO_4 were analyzed under the assumption that the SiO_2-Al_2O_3 matrix remains inert, allowing the topochemical dissolution of Y^{3+} ions without significant particle shrinkage. The process is likely controlled by mass transfer (either H_2SO_4 or Y^{3+} diffusion through a boundary layer or product deposit). This assumption is chemically justified as amorphous silica (as observed by XRF and XRD) exhibits extremely low solubility and dissolution kinetics in sulfuric acid due to the high stability of the Si-O-Si network and the formation of a protective, polynuclear layer of hydrated silica on the surface [35]. Similarly, aluminum oxide is highly stable in non-complexing acidic media such as H_2SO_4, where it forms a passivating layer that reduces its dissolution rate [36].

Therefore, for liquid film-controlled kinetics, pseudo-first-order (Equation (3)) or pseudo-second-order (Equation (4)) models apply:

$$k_{app}t = -ln(1-x) \tag{3}$$

$$kt = (1-x)^{-1} \tag{4}$$

where x is the fraction of metal solubilized (dimensionless), t (min) is the reaction time, k_{app} (min^{-1}) is the pseudo-first-order kinetic constant, and k (min^{-1}) is the second-order constant. However, if product layer diffusion controls the kinetics, and the Zhuravlev–Leshokin–Templeman (Z-L-T) model (Equation (5)) applies, where k_d is the reaction constant (min^{-1}) [37]:

$$k_d t = \left(\left((1-x)^{-\frac{1}{3}}\right) - 1\right)^2 \tag{5}$$

For boundary layer-controlled kinetics, the process can be evaluated according to the shrinking core model proposed by Ginstling–Brounsthein (Equation (6)) and Jander for a spherical particle (Equation (7)) [38]:

$$k_{pl}t = 1 - \frac{2}{3}x - (1-x)^{\frac{2}{3}} \tag{6}$$

$$k_s t = \left(1 - (1-x)^{\frac{1}{3}}\right)^2 \tag{7}$$

where k_{pl} $\left(min^{-1}\right)$ is the apparent rate constant of the shrinking core model with an insoluble product layer, and k_s is the apparent rate constant for a spherical model. For all experiments shown in Figures 2 and 3, the rate constant values and correlation coefficients (R^2) were calculated using the corresponding models. Specifically, the effects of the solid–

liquid ratio (Table 5, Figure 2) and temperature (Table 6, Figure 3) were analyzed. Overall, the results showed a better fit with the Z-L-T model (Figure 3b).

Table 5. Kinetic constants for proposed models of yttrium extraction as a function of solid–liquid ratio and H_2SO_4 concentration at room temperature.

S/L(g/L)	$[H_2SO_4]$/N	Kinetic Model				
		Pseudo-First-Order	Second-Order	Z-L-T	Ginstling–Brounsthein	Jander
		k_{app}/min^{-1}	k/min^{-1}	k_d/min^{-1}	k_{pl}/min^{-1}	k_s/min^{-1}
		* Correlation Coefficient R^2				
0.25	1	2.955×10^{-4}	3.0393×10^{-4}	2.7095×10^{-6}	2.5117×10^{-6}	2.5596×10^{-6}
		* 0.9815	* 0.9788	* 0.9556	* 0.9572	* 0.9568
0.5	1	6.2060×10^{-4}	6.9713×10^{-4}	1.6992×10^{-5}	1.4144×10^{-5}	1.4805×10^{-5}
		* 0.9166	* 0.9334	* 0.9978	* 0.9959	* 0.9958
0.25	2	5.3930×10^{-4}	5.3930×10^{-4}	1.1970×10^{-5}	1.0219×10^{-5}	1.0628×10^{-5}
		* 0.9250	* 0.9250	* 0.9833	* 0.9832	* 0.9834
0.5	2	1.1663×10^{-3}	9.9237×10^{-4}	3.8515×10^{-5}	2.9766×10^{-5}	3.1725×10^{-5}
		* 0.9622	* 0.9507	* 0.9532	* 0.9432	* 0.9411

Table 6. Kinetic constants for proposed models of yttrium extraction as a function of temperature. S/L = 0.25 g/mL, $[H_2SO_4]$ = 2 M.

Temperature/ °C	Kinetic Model				
	Pseudo-First-Order	Second-Order	Z-L-T	Ginstling–Brounsthein	Jander
	k_{app}/min^{-1}	k/min^{-1}	k_d/min^{-1}	k_{pl}/min^{-1}	k_s/min^{-1}
	* Correlation Coefficient R^2				
35	1.5239×10^{-3}	1.1985×10^{-3}	7.2060×10^{-5}	4.9606×10^{-5}	25.4339×10^{-5}
	* 0.8683	* 0.8287	* 0.9686	* 0.9485	* 0.9541
45	1.2780×10^{-3}	1.6603×10^{-3}	8.7403×10^{-5}	5.6938×10^{-5}	6.3087×10^{-5}
	* 0.7735	* 0.8193	* 0.9545	* 0.9043	* 0.9124
55	1.3668×10^{-3}	1.8499×10^{-3}	1.068×10^{-4}	6.6897×10^{-5}	7.5081×10^{-5}
	* 0.7645	* 0.8294	* 0.9381	* 0.9166	* 0.9247
65	1.5440×10^{-3}	2.1391×10^{-3}	1.4015×10^{-4}	5.6938×10^{-5}	3.1725×10^{-5}
	* 0.7590	* 0.8320	* 0.9501	* 0.9043	* 0.9411

The Z-L-T model assumes that the reaction rate is directly proportional to the concentration of the reactant (H_2SO_4) and the surface area of the solid being leached. Furthermore, the reaction is controlled by diffusion through a porous product layer. The complex multi-component nature of the fluorescent lamp waste, containing significant amounts of calcium (15.9% as CaO), aluminum (18.6% as Al_2O_3), sodium (13.90% as Na_2O), and silicon (45.8% as SiO_2) as major constituents (Table 2), promotes the formation of mixed diffusion barriers. The high calcium and sodium content suggests that these elements will also leach. Considering the low solubility of calcium sulfate at high sulfate concentrations [39], combined with a porous silica-rich layer formed by glass matrix dissolution, a composite product layer that limits reagent diffusion is likely created. Furthermore, the solubility of rare earth sulfates decreases with increasing temperature [40,41]. This mechanism is consistent with the Z-L-T model, which effectively describes systems where diffusion through such porous product layers is rate-limiting.

Geometrically, the model assumes particles may exhibit spherical shapes or a regular morphology, with a defined size distribution. Additionally, the surface area of the particles remains constant, indicating that the core size does not change significantly during the reaction, as the primary phase remains unreacted. It is worth noting that this model has successfully been used to describe the leaching behavior of REE from zircon tailings using HCl [42], as well as terbium leaching from Lapindo mud with H_2SO_4 [37].

A detailed examination of the Z-L-T rate constants in Table 5 shows that k_d is highly sensitive to changes in the solid–liquid ratio (S/L). At 1 M H_2SO_4, reducing the S/L ratio from 0.5 to 0.25 g/L increased k_d by approximately one order of magnitude (from 1.6992×10^{-5} to 2.7095×10^{-6} min^{-1}). This enhancement demonstrates that the diffusion limitation is diminished when more acid volume is available per unit mass of solid, likely reducing the effective thickness and density of the product layer. Regarding acid concentration, increasing from 1 M to 2 M H_2SO_4 at constant S/L (0.25 g/L) increased k_d by a factor of 4.4 (from 2.7095×10^{-6} to 1.1970×10^{-5} min^{-1}). This substantial increase is less pronounced than the effect of S/L variation. This relationship strongly suggests that, while an increased acid concentration accelerates the interfacial reaction rate and strengthens the concentration gradient—which is the driving force for diffusion—the primary resistance remains the physical barrier of the product layer itself. Therefore, the composite layer's permeability appears to be the dominant controlling factor.

The temperature dependence of k_d (Table 6) shows an increase from 7.2060×10^{-5} to 1.4015×10^{-4} min^{-1} between 35 and 65 °C, representing an overall increase by a factor of 1.94. Although, as expected, there is an increase in the reaction rate, it can be considered small compared to that observed in chemically controlled reactions, which is an indirect corroboration that diffusion is the limiting factor. The calculated apparent activation energy of 35.5 kJ mol^{-1} (derived below) falls within the typical range for mixed diffusion-controlled processes, further corroborating that the transport of reagents through the possible composite $Na_2SO_4/CaSO_4/SiO_2$ layer, rather than the chemical reaction at the yttrium oxide surface, governs the overall leaching rate.

To provide experimental evidence supporting the formation of a sulfate-based diffusion layer, the solid residue after leaching was characterized by FTIR (Figure 5). The spectrum shows bands at 1140 cm^{-1} and 1024 cm^{-1}, which are unequivocally assigned to the asymmetric (ν_3) and symmetric (ν_1) stretching vibrations of the sulfate ion (SO_4^{2-}), respectively [43–45], while the band at 580 cm^{-1} may correspond to the ν_4 mode. The broad band at 3366 cm^{-1} and the sharp band at 1636 cm^{-1} are characteristic of O-H stretching and H-O-H bending vibrations of adsorbed crystalline water, suggesting the presence of hydrated sulfate phases. This FTIR profile confirms the significant formation of sulfate species on the solid residue after leaching.

To identify the chemical species precipitating from the leach solution—which are indicative of the reactions occurring at the solid–liquid interface—the leach liquor obtained under optimal conditions (2 M H_2SO_4, 65 °C) was evaporated to dryness, and the resulting solids were analyzed by Scanning Electron Microscopy with Energy Dispersive X-ray Spectroscopy (SEM-EDS). Figure 6a shows the heterogeneous morphology of the crystallized material, with three representative points selected for punctual EDS analysis (Table 7). The punctual EDS data reveal the distinct sulfate salts that precipitate from the leachate. Point 1 is dominated by sulfur (25.34 wt.%) and calcium (17.56 wt.%), suggesting the formation of $CaSO_4 \cdot H_2O$. The significant yttrium content (10.12 wt.%) at this location indicates the probable co-precipitation of yttrium sulfate [$Y_2(SO_4)_3$] with the dominant calcium sulfate phase, explaining the low overall efficiency. Point 2 shows a strong association between sulfur (26.24 wt.%) and sodium (19.48 wt.%), characteristic of sodium sulfate, Na_2SO_4, which originates from the extensive leaching of sodium from the glass matrix (13.9% Na_2O, Table 2). Point 3 represents a more complex aggregate, with moderate sulfur (18.90 wt.%), significant sodium, and various other cations (Cu, Zn, Fe, Al), reflecting the multi-component nature of the waste and the formation of mixed sulfate salts.

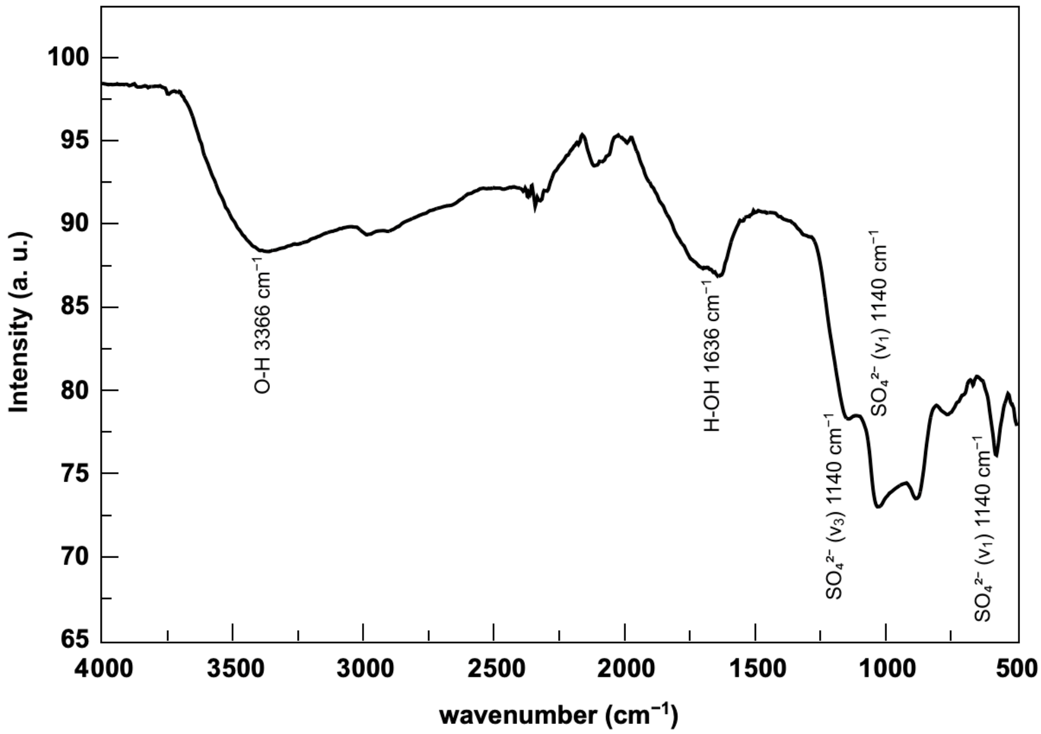

Figure 5. FTIR spectra from solid waste products after leaching.

Table 7. Punctual EDS composition (weight %) of phases in dried leachate (Figure 6a).

Element	Point 1	Point 2	Point 3
O	42.17	52.05	54.45
Na	1.92	19.48	9.36
Mg	0.17	-	1.28
Al	0.67	0.15	0.50
Si	-	0.06	1.33
P	-	0.65	-
S	25.34	26.24	18.90
Ca	17.56	-	1.46
Mn	0.33	-	-
Fe	0.78	0.61	3.11
Cu	0.94	0.75	5.23
Zn	-	-	4.38
Y	10.12	-	-

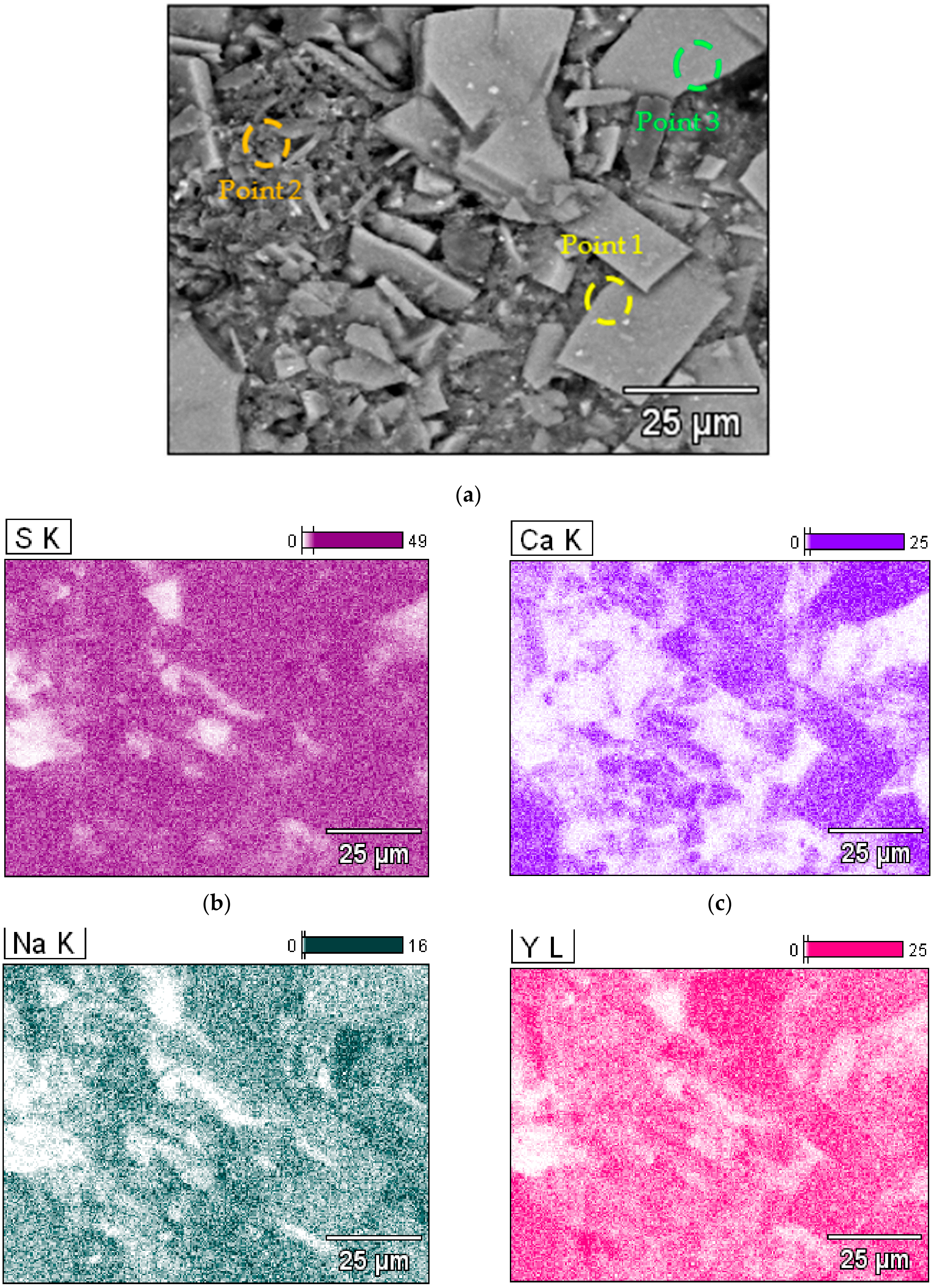

(**a**) (**b**) (**c**) (**d**) (**e**)

Figure 6. Characterization of the crystallized solids from the evaporated leach liquor: (**a**) representative SEM micrograph showing the heterogeneous morphology, with numbered points corresponding to punctual EDS analyses detailed in Table 7; and elemental distribution maps for (**b**) sulfur (S), (**c**) calcium (Ca), (**d**) sodium (Na), and (**e**) yttrium (Y).

Elemental mapping (Figure 6b–e) shows the distribution of these elements. The sulfur (S) map (Figure 6b) is prevalent, confirming sulfate as the dominant anionic species in the precipitate. The calcium (Ca) map (Figure 6c) and sodium (Na) map (Figure 6d) visually confirm the segregation into Ca-rich sulfate and Na-rich sulfate phases. The yttrium (Y) map (Figure 6e) is concentrated in the same areas as calcium. This provides direct visual evidence for the association of yttrium with the calcium sulfate phase, likely as a co-precipitate or adsorbed complex.

This analytical evidence supports the precipitation of sulfate salts in situ during the leaching process, forming a porous but obstructive layer. The probable co-precipitation of yttrium sulfate within this layer further reduces the driving force for yttrium dissolution. These phenomena synergistically create a diffusion barrier that controls the rate of ion transport, consistent with the product-layer diffusion mechanism described by the Z-L-T model. Moreover, the identification of sodium sulfate further confirms the leaching of major glass components, which contributes to the porosity and specific properties of the diffusion-controlling layer.

For reactions where the rate is sufficiently high, the apparent activation energy can be calculated using the Arrhenius equation (Equation (8)):

$$lnk_d = -\frac{E_a}{RT} + lnA \tag{8}$$

where k_d is the rate constant (from the Z-L-T shrinking core model), R is the ideal gas constant, T is the absolute temperature of the reaction, E_a is the apparent activation energy, and A is the pre-exponential factor. Therefore, a plot of T^{-1} vs. $\ln k_{pl}$ can be used to calculate the activation energy, as seen in Figure 7. The apparent activation energy value determined in this study is 35.5 kJ mol^{-1} (8.04 kcal mol^{-1}). This value further supports a diffusion-controlled mechanism, as it falls within the characteristic range for processes limited by diffusion through product layers.

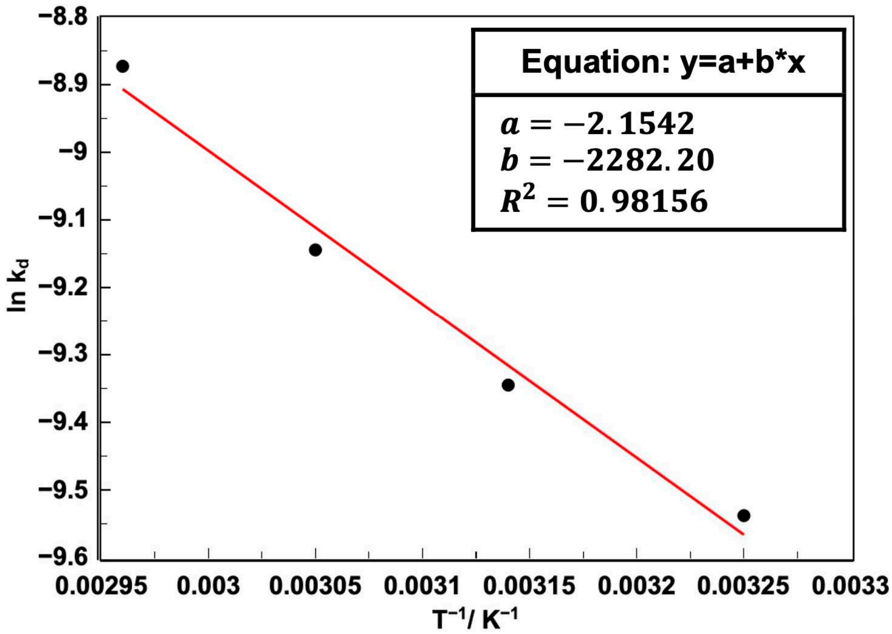

Figure 7. Arrhenius plot for fluorescent waste leaching.

2.3. [Y] Extraction from XAD-7 Resin

2.3.1. Effect of pH

The effect of pH on the extraction process was evaluated by adding controlled volumes of the leach liquor at a fixed concentration while maintaining a constant amount of XAD-7 resin, as shown in Figure 8. The solution pH was adjusted from 0.5 to 2.7. Studies on the sorption of rare earth elements (REE^{3+}) onto D_2EHPA-impregnated Amberlite XAD-7 resin show a strong pH dependence. The maximum extraction efficiency is reached within the pH range of 0.77 to 0.88, which agrees with the $pH_{\frac{1}{2}}$ value of the system, estimated at 0.8. This value corresponds to the point at which 50% of the REE^{3+} ions are transferred from the aqueous to the solid phase and serves as a reference to evaluate the efficiency of the sorption system.

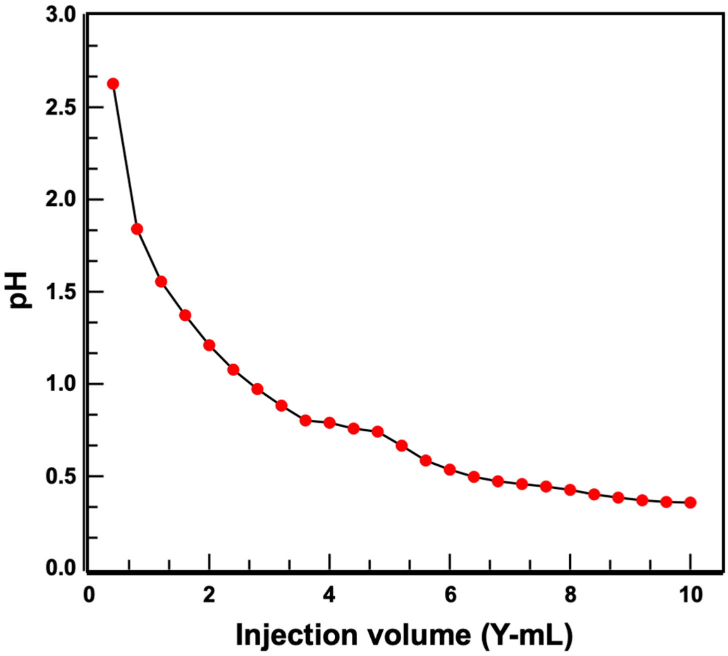

Figure 8. Effect of pH on yttrium extraction using D_2EHPA-impregnated XAD-7 resin. (solid–liquid ratio: 0.1 g/mL; yttrium solution: 44.2%).

Below pH 0.8, the sorption capacity of the resin increases significantly. This behavior is explained by the progressive deprotonation of the phosphate groups of D_2EHPA, which act as chelating agents. Once deprotonated, these functional groups exhibit a high affinity for REE^{3+} ions, facilitating the formation of stable complexes through coordinated interactions. Sorption occurs through both complex formation and physicochemical adsorption mechanisms, which increase the overall yield of the process [46,47].

From Figure 9, it was determined that at pH 0.75, the sorption capacity reached its maximum, with extraction rates above 90% for yttrium [Y]. This result confirms that acidic conditions favor the interaction between the impregnated extractant and the metal ions in solution. In contrast, as the pH increased above 0.8, the sorption efficiency decreased markedly. This effect is attributed to changes in the chemical equilibrium of REE^{3+} species in the aqueous phase, where the formation of hydroxylated species or less reactive aqueous complexes reduces their affinity towards the active sites of the extractant.

Therefore, the efficiency of the extraction process using Amberlite XAD-7 resin impregnated with D_2EHPA is strongly dependent on the solution pH. The optimum condition is just below $pH_{\frac{1}{2}} \approx 0.8$, where the complexation and adsorption mechanisms operate synergistically to maximize the extraction of rare earth ions. Thus, this pH value was used in all subsequent extraction processes.

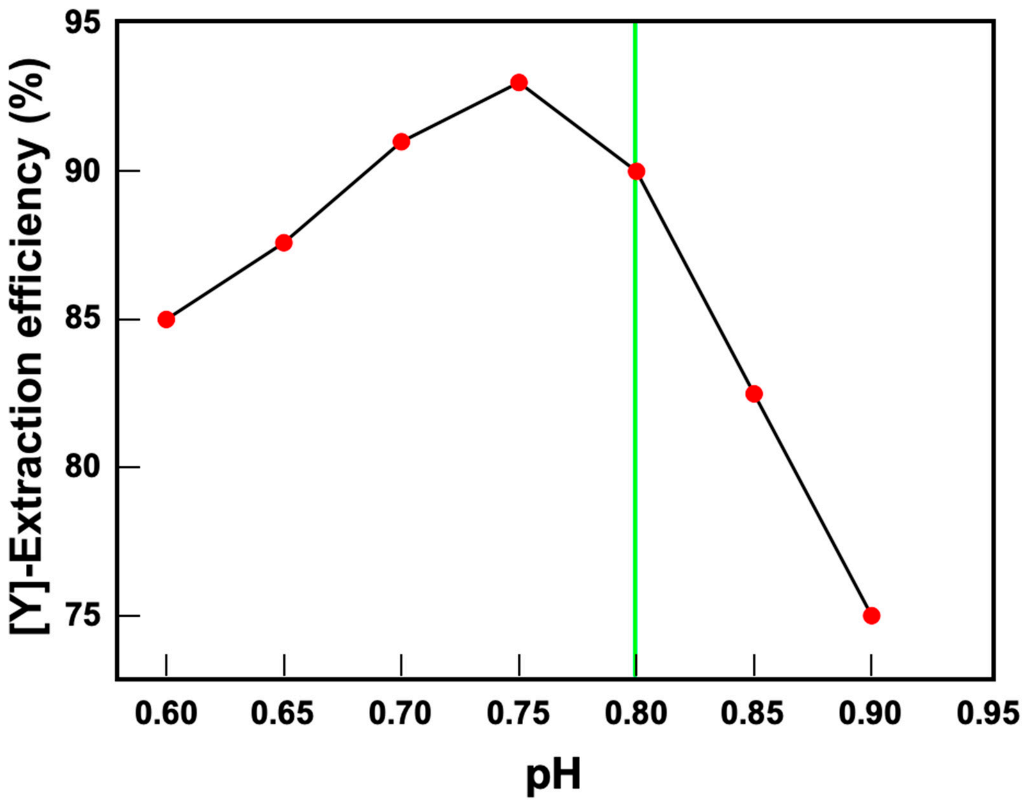

Figure 9. Relationship between pH and S-L extraction efficiency of REE^{3+} with XAD-7 resins impregnated with D_2EHPA.

2.3.2. Extraction Process

The extractions were performed by varying the resin dosage (1, 1.5, and 2 g) of solvent-impregnated resin (SIR) functionalized with 20% D_2EHPA and 80% kerosene, while maintaining the same volume of leached liquor (10 mL) for 2 h. Figure 10 shows a schematic of the interaction between the resin particles and the metal ions during the extraction. For comparison, the liquid–liquid extractions were also performed with the same extractant mixture (D_2EHPA–kerosene), corresponding to the amount used in the solid–liquid process. Figure 11 shows the results of these extractions. The bars represent the solid–liquid extraction, and recovery above 99% is observed in all three cases, regardless of the amount of resin added.

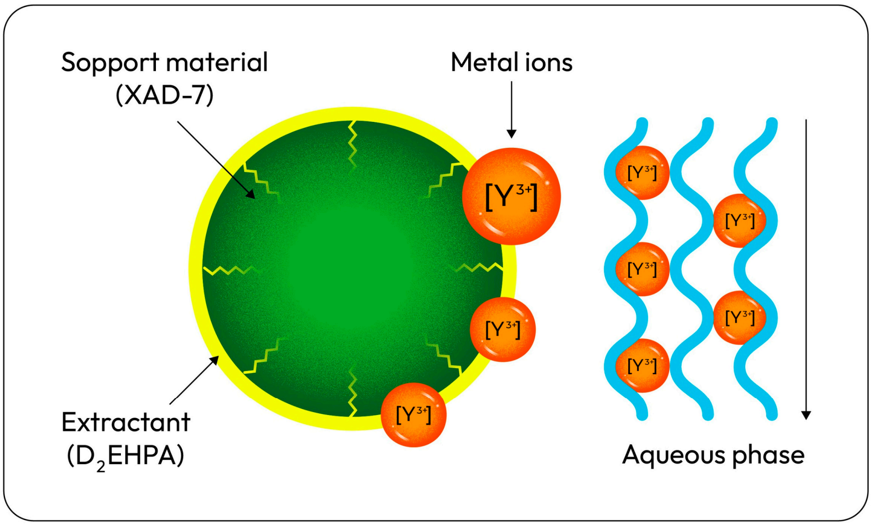

Figure 10. Theoretical scheme of yttrium extraction by functional particles.

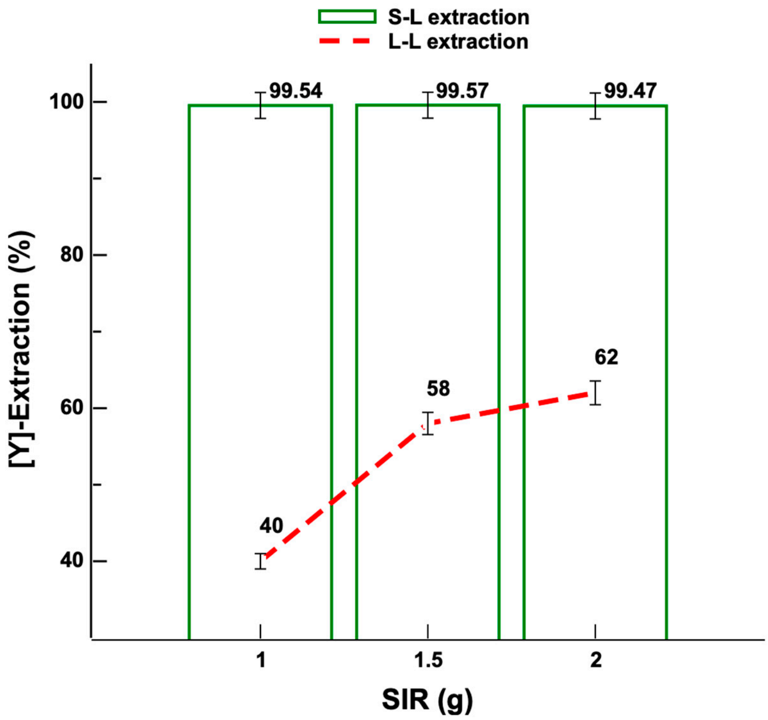

Figure 11. Comparison between solid–liquid and liquid–liquid extraction processes: SIR functionalized with 20% D_2EHPA and 80% kerosene; 44.2% initial concentrated yttrium solution.

Increasing the amount of resin used in the extraction process (1, 1.5, and 2 g), the surface area increases; therefore, the contact area between the yttrium ions and the extractant is greater, resulting in higher efficiency recovery. When comparing this process with a liquid–liquid extraction mechanism in which the contact area is limited by the interfacial area, the extraction efficiency is up to 50% lower, even with the same amount of extractant as in the resin process. This shows that the solid–liquid process is efficient for the recovery of yttrium. The extraction of trivalent rare earth ions with extractants such as D_2EHPA by the equilibrium in Equation (9) [48]:

$$M^{3+} + 3HD \leftrightarrow MD_3 + 3H^+ \tag{9}$$

where M is any REE cation, and D is the organic anion.

During extraction, the functional groups of D_2EHPA are deprotonated, favoring the formation of stable dimeric structures that lead to the formation of pseudo-chelates [49].

2.3.3. Stripping

The recovery process was completed by stripping the resin after extraction. Figure 12 compares the extraction and stripping yields. The stripping process was performed in a single stage at pH 2, yielding a recovery of 21% of the total amount extracted (99%). As shown in Figure 12, the single-stage stripping process achieved only 21% yttrium recovery, so a stepwise stripping process was performed. The process consisted of five stages with the same loaded resin, with each step lasting 120 min; the results are shown in Table 8. The aim was to determine how many steps were necessary to release the maximum amount of yttrium from the resins.

https://doi.org/10.3390/recycling11010022

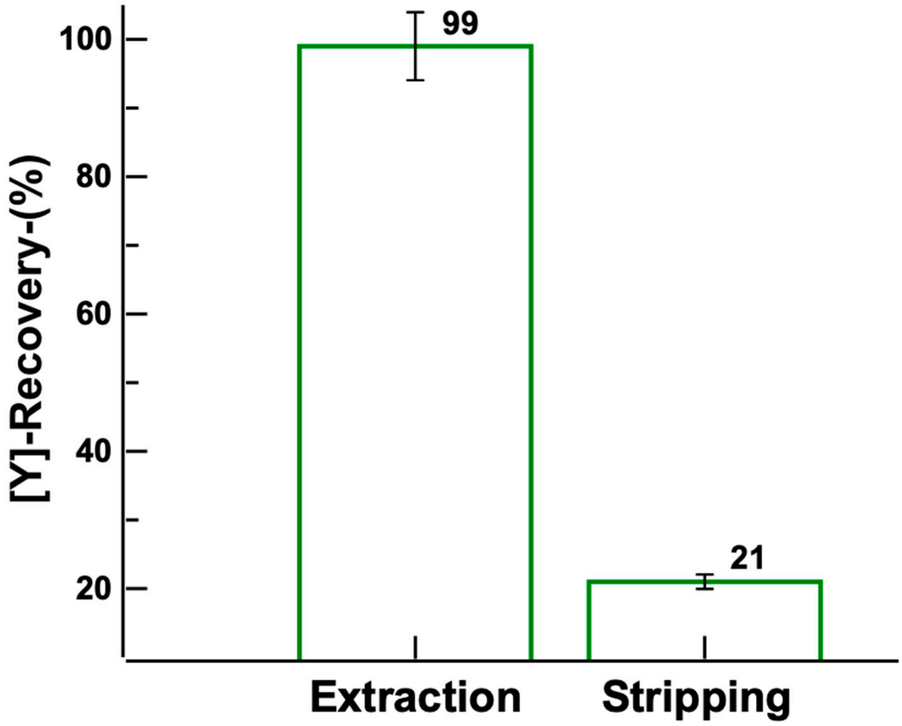

Figure 12. Comparison between extraction and stripping processes: SIR functionalized with 20% D_2EHPA and 80% kerosene at 0.1 g/mL. Initial yttrium solution concentration: 44.2%.

Table 8. Yttrium stripping results by step. Initial yttrium solution concentration: 461.90 mg/L. Solid–liquid ratio: 0.1 g/mL.

Stripping Step	Process Time	SIR (g)	% Stripping	% Remaining	% Efficiency per Step	% Accumulative Stripping	[Y] (mg/L)	Concentration of [Y] at Each Stage per Accumulated Volume (mg/L)
1	120 min	0.1 g/mL	21.11	77.89	21.32	21.11	97.50	97.50
2			20.16	57.73	25.88	41.27	93.11	95.31
3			20.9	36.83	36.20	62.17	96.53	95.72
4			19.27	17.56	65.28	81.44	89.00	94.04
5			16.33	1.23	92.99	97.77	75.42	90.31
Total stripping after 5 steps:							451.59 mg/L	

The stripping percentage and the concentration of yttrium recovered in each stage were recorded until more than 70% metal release was achieved. In the first stage, the stripping percentage was 21.11%, corresponding to 97.50 mg/L of yttrium. This initial stage represents a partial release, characteristic of systems involving strong chelating extractants, such as D_2EHPA, and is attributed to the high stability of the Y^{3+}-D_2EHPA complex and the kinetic limitations in disrupting these coordination bonds during the initial contact with the stripping agent. The gradual, multi-stage approach allows for progressive breakdown of the metal–extractant complexes and more complete recovery of yttrium. In the intermediate stages (Step 2 to Step 4), the cumulative stripping percentage increases significantly, reaching 83.27% in the second stage and 97.40% in the fourth stage (cumulative stripping percentage). Although the recovery continues to increase, the incremental efficiency of each stage decreases slightly, as less [Y] remains to be released. Finally, in the last stage, the cumulative stripping percentage is 97.77% (almost complete), with a [Y] concentration of 451.59 mg/L.

The stripping process appears to approach an equilibrium or saturation point, where significant improvement in recovery is no longer achieved, and the extracted concentration tends to stabilize, indicating that the process is cumulative and efficient, with a gradual decrease in [Y] concentration per stripping stage as less yttrium is available. The behavior is typical of a multi-stage stripping process with high efficiency at the beginning and decreasing yield in later stages [50].

2.4. Cycle Extraction

Five extraction and stripping cycles were performed with the same functionalized resin. The results are shown in Figure 13. The graph shows that yttrium recovery ([Y]-Recovery) remains very high and stable (between 95 and 99%) throughout five cycles, indicating excellent reusability of the material without significant loss of extraction efficiency. In contrast, the single-cycle stripping percentage remains relatively low (between 16 and 22%) and shows a slight decrease with cycles, suggesting that the stripping stage is incomplete. This implies that the material is highly selective and stable for Y extraction, but that the discharge process requires optimization (adjustments in pH, stripping medium, or operating conditions) to improve overall yttrium recovery.

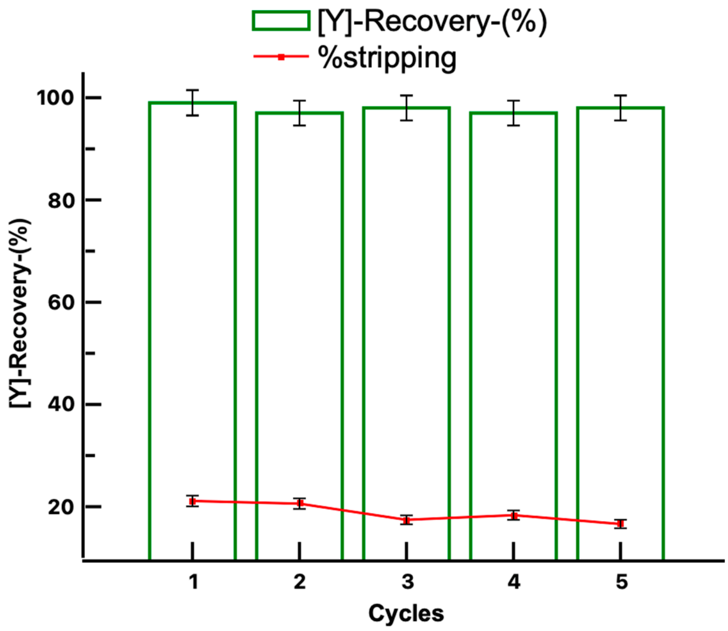

Figure 13. Extraction and stripping process by cycles with the same resin: SIR functionalized with 20% D_2EHPA and 80% kerosene at 0.1 g/mL; time per step: 120 min. Initial yttrium solution concentration: 44.2%.

2.5. Cost Analysis

The estimated cost of obtaining the functionalized resin for the yttrium recovery process from fluorescent lamp waste was taken from previous studies [14] and updated (Tables 9 and 10). To align the cost evaluation with standard industrial metrics, the operational cost is normalized to the amount of yttrium oxide (Y_2O_3) recovered per liter of leachate. From the leaching stage, approximately 45 g of $Y_2(SO_4)_3$ are obtained per liter, which corresponds to 21.6 g of theoretically available Y_2O_3. With an overall recovery efficiency of 43%, the effective yield is 9.29 g of Y_2O_3 per liter of leachate.

Table 9. Cost of the extractant-impregnated resin process.

Cost of Resin and Solvents			
Reagent	**Quantity**	**Unit Price**	**Cost**
Original Amberlite® XAD-7	100 g	30 USD/kg	3 USD
D_2EHPA	200 mL	4.5 USD/L	0.9 USD
Kerosene	800 mL	0.8–1 USD/L	0.8 USD
Ethanol	100 mL	1–1.5 USD/L	0.125 USD
Water	5000 mL	0.70 USD/m^3	0.00035 USD
Unit cost of electricity (México, 2025)			0.05 USD/kWh
(a) Cost of resin impregnation at 20% D_2EHPA in kerosene Power of magnetic stirrer in kWh × electricity cost per unit + reagents			
(b) Cost of drying in the oven Power of oven in kWh× electricity cost per unit + after washing + after impregnation			
Total cost: Cost incurred = (a) + (b)		4.87 USD	

Table 10. Cost of leaching process [14].

Cost of Leaching Fluorescent Lamps			
Reagent	**Quantity**	**Unit Price**	**Cost**
H_2SO_4	1000 mL	0.18 USD/L	0.18 USD
Water	500 mL	0.70 USD/m^3	0.00035 USD
Unit cost of electricity (México, 2025)		0.05 USD/kWh	0.05 USD/kWh
(a) Waste grinding cost Ball mill (kWh) × electricity cost per unit			
(b) Cost of leaching fluorescent lamps (S/L = 0.25 g/mL and 2 M H_2SO_4) Power of magnetic stirrer in kWh × electricity cost per unit + reagents			
Total cost: Cost incurred= (a) + (b)		0.23 USD	

The leaching stage has an operational cost of 0.23 USD per liter, while the secondary extraction step using the functionalized resin requires 4.87 USD per 100 g of resin. Considering that the impregnated resin can be reused for five consecutive cycles, the amortized resin cost decreases to 0.97 USD per cycle.

Therefore, the total operational expenditure (OPEX) amounts to approximately 1.20 USD per liter of leachate, including both leaching and extraction stages. Based on a production yield of 9.29 g of Y_2O_3 per liter, the resulting production cost is approximately 129.17 USD per kilogram of Y_2O_3. The updated analysis demonstrates that the production cost is approximately 129.17 USD per kg of Y_2O_3 when resin reuse is considered, which is within the commercially viable range.

3. Materials and Methods

3.1. Loss on Ignition (LOI)

LOI tests were performed at 700 °C in a Barnstead Thermolyne (Waltham, Massachusetts, USA) muffle furnace for 2 h. The initial weight was 100.0004 g, and the final weight was 90.9578 g.

3.2. Leaching of Fluorescent Lamps

Tubular fluorescent lamps of different wattages and lengths (21 W—849 mm, 30 W—895 mm, 23 W—970 mm, 36 W—1200 mm, 58 W—1500 mm) were used. The ballasts and metal terminals, composed mainly of copper and steel, were removed manually. A controlled incision was made in each tube, and a suction system was immediately attached to capture the released mercury vapor, which was retained in an aqueous solution to prevent its release into the environment. Subsequently, the tube fragments were introduced into a ball mill, using steel spheres with diameters between 5 and 10 cm, and ground for 60 min. At the end of this stage, the resulting material was sieved, with an average particle size of 0.18 mm. The collected powder, composed of a mixture of glass and tricolor phosphors (red, green, and blue) characteristic of this type of lamp, was subjected to a leaching process. This stage was applied exclusively to the pulverized material from the milling.

For hydrometallurgical operations and selected REE separations, the fluorescent powder was leached with sulfuric acid (Fermont, Monterrey, México, 98%). Three different solid–liquid ratios were tested during the leaching process: 1:1, 1:2, and 1:4, with 250 g fluorescent powder/liter of leaching solution. Complete leaching was carried out in a single step using two different sulfuric acid concentrations (1 and 2 mol/L) at 25, 35, 45, 55, and 65 °C under normal pressure for 24 h. This process was carried out in a 1 L glass reactor with a vertical mixer and a simple 4-blade propeller.

For the kinetic analysis, 10 mL samples were taken at 15, 30, 45, 60, 90, 180, 240, and 300 min, without removing any solids. After sampling, 10 mL of acid solution was added to maintain the S/L ratio. Each sample was diluted with deionized water for subsequent analysis by ICP-MS.

3.3. Pre-Treatment of Resins

XAD-7 microsphere resin was used (Amberlite, Sigma-Aldrich, St. Louis, MO, USA). It was weighed, then immersed in distilled water, subjected to an ultrasonic bath to remove any remaining organic residues, and washed three times with deionized water. Finally, it was washed with ethanol and subsequently dried in an oven at 60 °C. They were impregnated with the D_2EHPA–kerosene solution (hydrogen phosphate, Sigma-Aldrich, St. Louis, MO, USA, 97%). The mixture was prepared at a ratio of 10 mL of organic solution (20% D2EHPA) per 1 g of clean, dry resin. The details of the resin functionalization have been reported previously [14]. Correct functionalization of the resin with D_2EHPA requires a thorough cleaning process. By means of weight difference and semiquantitative analysis by scanning electron microscopy (SEM), the extractant was shown to be securely adhered to the resin, both inside and on the surface, as reported in previous work [14]. Figure 14 shows a micrograph of the XAD-7 resin ready for the extraction process.

Table 11 shows the results obtained by EDS, which confirm the presence of phosphorus in the resin after the functionalization process, a characteristic element of the extractant (D_2EHPA) deposited on the particle surface.

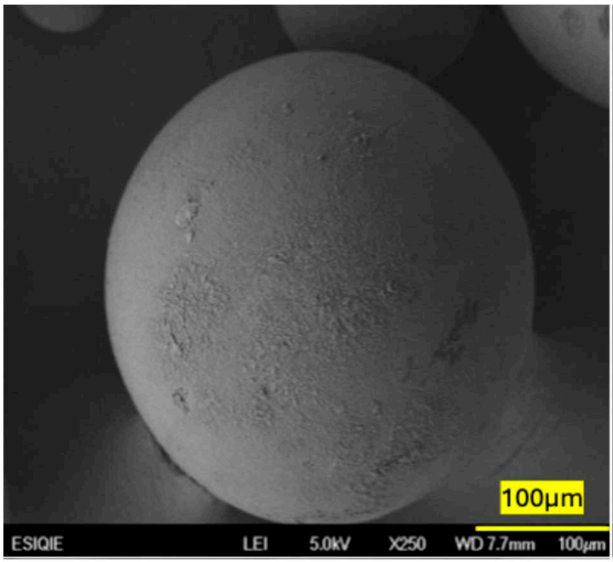

Figure 14. XAD-7 resin impregnated with D_2EHPA is ready for the extraction process.

Table 11. Chemical resin composition before and after functionalization.

	Element	Wt.%	Atomic %
Clean resin	C	63.74	70.43
	O	35.24	29.23
	Ca	1.02	0.34
Resin after functionalization with D_2EHPA	C	65.20	72.37
	O	31.41	26.17
	P	3.39	1.46

3.4. Solid–Liquid Extraction Process and Stripping

The solid–liquid extraction process was performed with the solution obtained from the leaching of fluorescent lamps. The initial REE concentrations are presented in Table 3. All extraction and stripping experiments were performed in triplicate, producing results with an average error of less than 2%.

For extraction, the solvent-impregnated resin (SIR) was added to the leaching solution. Three different S/L ratios were tested: 1, 1.5, and 2 (g/mL) to 20 vol% of D_2EHPA. A 450 r/min agitation was applied for 120 min. At the end of the extraction, the solid phase (resin loaded with metal ions) was separated from the aqueous surplus by filtration using size 42 ashless filter paper. A 2 mol/L sulfuric acid solution was prepared for the stripping. The S/L ratio for stripping was the same as that used in the 120 min extraction stage, with constant agitation at 450 r/min at room temperature.

The cyclic extraction was carried out using the same lot of functionalized resin under the optimal extraction and desorption conditions (S/L 0.1 g/L, 450 rpm at room temperature, and 120 min per step).

3.5. Sample Preparation and Analysis

Quantification of the metal concentration was performed using a PerkinElmer® Optima™ 8300 benchtop Inductively Coupled Plasma Optical Emission Spectrometer (ICP-OES, Springfield, IL, USA). For complete digestion, a 1:10 mL sample was used, and the samples from each leaching step were diluted 0.25:10 mL, as were the samples at each kinetic time point (15, 30, 45, 60, 90, 180, 240, 300 min), with the extracted volume being replaced. During the extractions, the samples taken were diluted 1:10 mL. All samples were filtered using size 42 ashless filter paper and made up to volume with ultrapure water.

3.6. Apparatus

The leaching process was conducted at 300 rpm using a conventional stirrer. The extraction and stripping stages were performed under constant agitation using a magnetic hot plate stirrer (Thermolyne, Mirak TM, USA). SEM images and EDS analysis were obtained using a SEM (JEOL JSM-7800F, Akishima, Tokio, Japan). Yttrium chemical analysis was performed using a PerkinElmer Optima 8300, a benchtop inductively coupled plasma–mass spectrometer (ICP-OES, Springfield, IL, USA). The functional groups present in the solid residues were identified by Fourier-Transform Infrared (FTIR) spectroscopy using a PERKIN ELMER FTIR 2000 spectrometer (FTIR, Springfield, IL, USA). The morphology and elemental composition of the leachate precipitates and resin were examined by Scanning Electron Microscopy with Energy Dispersive X-ray Spectroscopy (SEM-EDS) using a JEOL JSM-6300 microscope (Akishima, Tokyo, Japan).

4. Conclusions

This study successfully demonstrated an integrated hydrometallurgical process for the recovery of yttrium from spent fluorescent lamps. The process comprises three key stages: (1) multi-stage sulfuric acid leaching under optimized conditions (2 M, 65 °C, S/L 0.25 g/L) to dissolve yttrium from the phosphor matrix; (2) solid–liquid extraction of the clarified leachate using D2EHPA-impregnated Amberlite XAD-7 resin at pH 0.75 for selective yttrium recovery (>99%); and (3) multi-stage stripping with sulfuric acid to desorb and concentrate yttrium, regenerating the resin for reuse. The optimal leaching conditions achieved a yttrium dissolution efficiency of 44.2% per stage, with a cumulative recovery of 71.11% over four stages. Crucially, kinetic analysis coupled with FTIR and SEM-EDS characterization provided evidence that the leaching kinetics are governed by diffusion through a composite layer of precipitated calcium and sodium sulfates. This phenomenon, validated by the excellent fit of the Z-L-T model (Ea = 35.5 kJ mol^{-1}), explains the decelerating dissolution profile.

The solid–liquid extraction process using Amberlite XAD-7 resin impregnated with D_2EHPA proved to be highly effective and superior to conventional liquid–liquid extraction. A critical pH dependence was identified, with maximum yttrium extraction efficiency exceeding 99% at pH 0.75. This system demonstrated remarkable efficiency even at a low resin dosage (0.1 g/L), highlighting the advantage of the increased surface area provided by the solid support. Furthermore, the multi-stage stripping process with sulfuric acid confirmed the reusability and stability of the solvent-impregnated resins, achieving cumulative yttrium recovery of over 97% across five consecutive cycles, with an average stripping efficiency of 78.6% per cycle. Therefore, the combination of acid leaching and solid–liquid extraction with D_2EHPA-impregnated XAD-7 resin presents a viable, efficient, and more sustainable method for yttrium recovery from electronic waste. This approach not only mitigates the environmental impact of fluorescent lamp disposal but also enhances the security of supply for yttrium recovery.

Author Contributions: P.A.M.-M. and T.d.R.J.-R.: investigation, methodology, writing—original draft preparation; M.C.-T. and J.L.G.-E.: investigation; R.G.S.-A. and M.G.-H.: writing—review and editing; A.d.J.M.-R.: investigation, data curation, supervision, writing—original draft preparation. All authors have read and agreed to the published version of the manuscript.

Funding: Foundation item: Project supported by Secretariat of Research and Postgraduate Studies, National Polytechnic Institute by the 2389 multidisciplinary project (20251162, 20253472, and 20250704), and Secretaría de Ciencia, Humanidades, Tecnología e Innovación (Secihti).

Data Availability Statement: The original contributions presented in this study are included in the article. Further inquiries can be directed to the corresponding author.

Acknowledgments: The authors acknowledge Comisión de Fomento a las Actividades Académicas, Estimulo al desempeño de los Investigadores; Sistema Nacional de Investigadores, Secretaria de Ciencia, Humanidades, Tecnología e Innovación (SECIHTI) México; and the Instituto Politécnico Nacional—SIP.

Conflicts of Interest: The authors declare that they have no known competing financial interests or personal relationships that could have appeared to influence the work reported in this paper.

Abbreviations

The following abbreviations are used in this manuscript:

REEs	Rare earth elements
SIR	Solvent-impregnated resins
LRE	Light rare earths
D_2EHPA	Di-(2-ethylhexyl) phosphoric acid

References

1. Wells, W.H.; Wells, V.L. The Lanthanides, Rare Earth Elements. In *Patty's Toxicology*; John Wiley & Sons, Inc.: Hoboken, NJ, USA, 2012. [CrossRef]
2. Golloch, A. *Handbook of Rare Earth Elements: Analytics*; De Gruyter: Berlin, Germany, 2017.
3. Ursache, A. Critical materials raw as leverage in global geopolitics. *Sci. MORALITAS-Int. J. Multidiscip. Res.* **2023**, *8*, 239–250. [CrossRef]
4. Dhawan, N.; Tanvar, H. A critical review of end-of-life fluorescent lamps recycling for recovery of rare earth values. *Sustain. Mater. Technol.* **2022**, *32*, e00401. [CrossRef]
5. Lukowiak, A.; Zur, L.; Tomala, R.; LamTran, T.N.; Bouajaj, A.; Strek, W.; Righini, G.C.; Wickleder, M.; Ferrari, M. Rare earth elements and urban mines: Critical strategies for sustainable development. *Ceram Int.* **2020**, *46*, 26247–26250. [CrossRef]
6. Xavier, L.H.; Ottoni, M.; Abreu, L.P.P. A comprehensive review of urban mining and the value recovery from e-waste materials. *Resour. Conserv. Recycl.* **2023**, *190*, 106840. [CrossRef]
7. Binnemans, K.; Jones, P.T.; Blanpain, B.; Van Gerven, T.; Yang, Y.; Walton, A.; Buchert, M. Recycling of rare earths: A critical review. *J. Clean. Prod.* **2013**, *51*, 1–22. [CrossRef]
8. Pavón, S.; Lapo, B.; Fortuny, A.; Sastre, A.M.; Bertau, M. Recycling of rare earths from fluorescent lamp waste by the integration of solid-state chlorination, leaching and solvent extraction processes. *Sep. Purif. Technol.* **2021**, *272*, 118879. [CrossRef]
9. Mishra, B.B.; Devi, N.; Sarangi, K. Yttrium and europium recycling from phosphor powder of waste tube light by combined route of hydrometallurgy and chemical reduction. *Miner. Eng.* **2019**, *136*, 43–49. [CrossRef]
10. Saratale, R.G.; Kim, H.-Y.; Park, Y.; Shin, H.S.; Ghodake, G.; Bharagava, R.N.; Mulla, S.I.; Kim, D.-S.; Saratale, G.D. Hydrometallurgical process for the recovery of yttrium from spent fluorescent lamp: Leaching and crystallization experiments. *J. Clean. Prod.* **2020**, *261*, 121009. [CrossRef]
11. Schaeffer, N.; Feng, X.; Grimes, S.; Cheeseman, C. Recovery of an yttrium europium oxide phosphor from waste fluorescent tubes using a Brønsted acidic ionic liquid, 1-methylimidazolium hydrogen sulfate. *J. Chem. Technol. Biotechnol.* **2017**, *92*, 2731–2738. [CrossRef]
12. Quinn, J.E.; Soldenhoff, K.H.; Stevens, G.W.; Lengkeek, N.A. Solvent extraction of rare earth elements using phosphonic/phosphinic acid mixtures. *Hydrometallurgy* **2015**, *157*, 298–305. [CrossRef]
13. Tunsu, C.; Lapp, J.B.; Ekberg, C.; Retegan, T. Selective separation of yttrium and europium using Cyanex 572 for applications in fluorescent lamp waste processing. *Hydrometallurgy* **2016**, *166*, 98–106. [CrossRef]
14. Martínez-Montoya, P.A.; Sanchez-Alvarado, R.G.; Medina-Velazquez, D.Y.; Carrera-Jota, M.L.; Garnica-Chávez, P.; de J. Morales-Ramirez, A. Solid-liquid extraction for yttrium recovery using porous polymeric resin (XAD-7) functionalized with D2EHPA. *J. Rare Earths* **2023**, *42*, 1764–1773. [CrossRef]

15. Wu, S.; Wang, L.; Zhang, P.; El-Shall, H.; Moudgil, B.; Huang, X.; Zhao, L.; Zhang, L.; Feng, Z. Simultaneous recovery of rare earths and uranium from wet process phosphoric acid using solvent extraction with D2EHPA. *Hydrometallurgy* **2018**, *175*, 109–116. [CrossRef]
16. Hidayah, N.N.; Abidin, S.Z. The evolution of mineral processing in extraction of rare earth elements using solid-liquid extraction over liquid-liquid extraction: A review. *Miner. Eng.* **2017**, *112*, 103–113. [CrossRef]
17. Reddy, B.R.; Kumar, B.N.; Radhika, S. Solid-Liquid extraction of terbium from phosphoric acid medium using bifunctional phosphinic acid resin, tulsion CH-96. *Solvent Extr. Ion Exch.* **2009**, *27*, 695–711. [CrossRef]
18. Sun, X.; Peng, B.; Ji, Y.; Chen, J.; Li, D. The solid-liquid extraction of yttrium from rare earths by solvent (ionic liquid) impreganated resin coupled with complexing method. *Sep. Purif. Technol.* **2008**, *63*, 61–68. [CrossRef]
19. Karve, M.; Pandey, K. Sorption studies of U (VI) on Amberlite XAD-2 resin impregnated with Cyanex272. *J. Radioanal. Nucl. Chem.* **2012**, *293*, 783–787. [CrossRef]
20. Yang, B.; Wu, S.; Liu, X.; Yan, Z.; Liu, Y.; Li, Q.; Yu, F.; Wang, J. Solid-phase extraction and separation of heavy rare earths from chloride media using P227-impregnated resins. *Rare Met.* **2021**, *40*, 2633–2644. [CrossRef]
21. Ciopec, M.; Davidescu, C.; Negrea, A.; Grozav, I.; Lupa, L.; Negrea, P.; Popa, A. Adsorption studies of Cr(III) ions from aqueous solutions by DEHPA impregnated onto Amberlite XAD7—Factorial design analysis. *Chem. Eng. Res. Des.* **2012**, *90*, 1660–1670. [CrossRef]
22. Draa, M.T.; Belaid, T.; Benamor, M. Extraction of Pb(II) by XAD7 impregnated resins with organophosphorus extractants (DEHPA, IONQUEST 801, CYANEX 272). *Sep. Purif. Technol.* **2004**, *40*, 77–86. [CrossRef]
23. Benamor, M.; Bouariche, Z.; Belaid, T.; Draa, M.T. Kinetic studies on cadmium ions by Amberlite XAD7 impregnated resins containing di(2-ethylhexyl) phosphoric acid as extractant. *Sep. Purif. Technol.* **2008**, *59*, 74–84. [CrossRef]
24. Negrea, A.; Ciopec, M.; Lupa, L.; Davidescu, C.M.; Popa, A.; Ilia, G.; Negrea, P. Removal of AsV by FeIII-loaded XAD7 impregnated resin containing Di(2-ethylhexyl) phosphoric acid (DEHPA): Equilibrium, kinetic, and thermodynamic modeling studies. *J. Chem. Eng. Data* **2011**, *56*, 3830–3838. [CrossRef]
25. İnan, S.; Tel, H.; Sert, Ş.; Çetinkaya, B.; Sengül, S.; Özkan, B.; Altaş, Y. Extraction and separation studies of rare earth elements using Cyanex 272 impregnated Amberlite XAD-7 resin. *Hydrometallurgy* **2018**, *181*, 156–163. [CrossRef]
26. Ciopec, M.; Davidescu, C.M.; Negrea, A.; Duţeanu, N.; Rusu, G.; Grad, O.; Negrea, P. Amberlite XAD7 resin functionalized with crown ether and Fe(III) used for arsenic removal from water. *Pure Appl. Chem.* **2018**, *91*, 375–388. [CrossRef]
27. Elbadawy, H.A.; Abdel-Salam, A.H.; Khalil, T.E. The impact of an Amberlite XAD-16-based chelating resin for the removal of aqueous Cd(II) and Pb(II)ions. *Microchem. J.* **2021**, *165*, 106097. [CrossRef]
28. Grad, O.A.; Ciopec, M.; Negrea, A.; Duteanu, N.; Negrea, P.; Vodă, R. Evaluation of performance of functionalized amberlite xad7 with dibenzo-18-crown ether-6 for palladium recovery. *Materials* **2021**, *14*, 1003. [CrossRef]
29. Yarahmadi, A.; Khani, M.H.; Zarandi, M.N.; Amini, Y. Ce(III) and La(III) ions adsorption through Amberlite XAD-7 resin impregnated via CYANEX-272 extractant. *Sci. Rep.* **2023**, *13*, 6930. [CrossRef] [PubMed]
30. Vancea, C.; Ciocarlie, L.; Negrea, A.; Mosoarca, G.; Ciopec, M.; Duteanu, N.; Negrea, P.; Pascu, B.; Nemes, N.-S. Evaluation of Functionalized Amberlite Type XAD7 Polymeric Resin with L-Valine Amino Acid Performance for Gallium Recovery. *Polymers* **2024**, *16*, 837. [CrossRef] [PubMed]
31. Chagnes, A.; Pospiech, B. A brief review on hydrometallurgical technologies for recycling spent lithium-ion batteries. *J. Chem. Technol. Biotechnol.* **2013**, *88*, 1191–1199. [CrossRef]
32. Demol, J.; Ho, E.; Soldenhoff, K.; Senanayake, G. The sulfuric acid bake and leach route for processing of rare earth ores and concentrates: A review. *Hydrometallurgy* **2019**, *188*, 123–139. [CrossRef]
33. Maina, L.; Kiegiel, K.; Samczyński, Z.; Haneklaus, N.; Zakrzewska-Kołtuniewicz, G. Sulfuric Acid Leaching Recovery of Rare Earth Elements from Wizów's Phosphogypsum in Poland. *Sustainability* **2024**, *16*, 9059. [CrossRef]
34. Sulaiman, M.Y.M. Rate of Rare Earths Leaching in HCl, H_2SO_4 and HNO_3. *Adv. Mat. Res.* **2013**, *795*, 1–4. [CrossRef]
35. Dove, P.M.; Nix, C.J. The influence of the alkaline earth cations, magnesium, calcium, and barium on the dissolution kinetics of quartz. *Geochim. Cosmochim. Acta* **1997**, *61*, 3329–3340. [CrossRef]
36. Zhang, S.; Zhu, W.; Li, Q.; Zhang, W.; Yi, X. Recycling of Secondary Aluminum Dross to Fabricate Porous γ-Al_2O_3 Assisted by Corn Straw as Biotemplate. *J. Mater. Sci. Chem. Eng.* **2019**, *7*, 87–102. [CrossRef]
37. Supriadi, H.; Suyanti, S.; Astuti, W.; Handini, T.; Sujoto, V.S.H.; Prameswara, G. Optimization and Kinetics of Terbium Leaching from Lapindo Mud using Sulfuric Acid as the Leaching Agent. *Bull. Chem. React. Eng. Catal.* **2025**, *20*, 35–43. [CrossRef]
38. Senanayake, G.; Das, G.K. A comparative study of leaching kinetics of limonitic laterite and synthetic iron oxides in sulfuric acid containing sulfur dioxide. *Hydrometallurgy* **2004**, *72*, 59–72. [CrossRef]
39. Zeng, D.; Wang, W. Solubility phenomena involving CaSO4 in hydrometallurgical processes concerning heavy metals. *Pure Appl. Chem.* **2011**, *83*, 1045–1061. [CrossRef]

40. Moldoveanu, G.A.; Kolliopoulos, G.; Judge, W.D.; Ng, K.L.; Azimi, G.; Papangelakis, V.G. Solubilities of individual light rare earth sulfates (lanthanum to europium) in water and H_2SO_4 solutions (neodymium sulfate). *Hydrometallurgy* **2024**, *223*, 106194. [CrossRef]
41. Zhang, S.G.; Yang, M.; Liu, H.; Pan, D.A.; Tian, J.J. Recovery of waste rare earth fluorescent powders by two steps acid leaching. *Rare Met.* **2013**, *32*, 609–615. [CrossRef]
42. Prameswara, G.; Trisnawati, I.; Mulyono, P.; Prasetya, A.; Petrus, H.T.B.M. Leaching Behaviour and Kinetic of Light and Heavy Rare Earth Elements (REE) from Zircon Tailings in Indonesia. *JOM* **2021**, *73*, 988–998. [CrossRef]
43. Marinova, D.; Wildner, M.; Bancheva, T.; Stoyanova, R.; Georgiev, M.; Stoilova, D.G. Synthesis, structure and properties of blödite-type solid solutions, $Na_2Co_1{-}xCux(SO_4)_24H_2O$ ($0 < x \leq 0.18$), and crystal structure of synthetic kröhnkite, $Na_2Cu(SO_4)_2{\cdot}2H_2O$. *Phys. Chem. Miner.* **2018**, *45*, 801–817. [CrossRef]
44. Radha, A.V.; Lander, L.; Rousse, G.; Tarascon, J.M.; Navrotsky, A. Thermodynamic stability and correlation with synthesis conditions, structure and phase transformations in orthorhombic and monoclinic $Li_2M(SO_4)_2$ (M = Mn, Fe, Co, Ni) polymorphs. *J. Mater. Chem. A Mater.* **2015**, *3*, 2601–2608. [CrossRef]
45. Kiefer, J.; Strk, A.; Kiefer, A.L.; Glade, H. Infrared spectroscopic analysis of the inorganic deposits from water in domestic and technical heat exchangers. *Energies* **2018**, *11*, 798. [CrossRef]
46. Metwally, S.S.; Hassan, M.A.; Aglan, R.F. Extraction of copper from ammoniacal solution using impregnated amberlite XAD-7 resin loaded with LIX-54. *J. Environ. Chem. Eng.* **2013**, *1*, 252–259. [CrossRef]
47. Lee, G.S.; Uchikoshi, M.; Mimura, K.; Isshiki, M. Separation of major impurities Ce, Pr, Nd, Sm, Al, Ca, Fe, and Zn from La using bis(2-ethylhexyl)phosphoric acid (D2EHPA)-impregnated resin in a hydrochloric acid medium. *Sep. Purif. Technol.* **2010**, *71*, 186–191. [CrossRef]
48. Ni'am, A.C.; Wang, Y.F.; Chen, S.W.; Chang, G.M.; You, S.J. Simultaneous recovery of rare earth elements from waste permanent magnets (WPMs) leach liquor by solvent extraction and hollow fiber supported liquid membrane. *Chem. Eng. Process.—Process Intensif.* **2020**, *148*, 107831. [CrossRef]
49. Wilson, A.M.; Bailey, P.J.; Tasker, P.A.; Turkington, J.R.; Grant, R.A.; Love, J.B. Solvent extraction: The coordination chemistry behind extractive metallurgy. *Chem. Soc. Rev.* **2013**, *43*, 123–134. [CrossRef]
50. Zielinski, S.; Buca, M.; Famulski, M. Precipitation-stripping processes for heavy metals. *Hydrometallurgy* **1998**, *48*, 253–263. [CrossRef]